Enhanced photocatalytic degradation of hydrolyzed polyacrylamide by three-dimensional Cu_2O/graphene@nickel foam composite

Zuchao Meng*, Chengxi Li, Mao Li, Qianding Li, Xiang Liu

College of Chemistry and Chemical Engineering, Xi'an Shiyou University, Xi'an 710065, Shaanxi, China, Tel./Fax: +86 29 88382693; emails: zcmeng@xsyu.edu.cn (Z. Meng), 386945807@qq.com (C. Li), 865381329@qq.com (M. Li), qdli@xsyu.edu.cn (Q. Li), lxhx@xsyu.edu.cn (X. Liu)

ABSTRACT

The three-dimensional (3D) Cu_2O/graphene@nickel foam (Cu_2O/GO@NF) photocatalyst was synthesized via a simple immersion-electrodeposition method. The as-prepared photocatalyst assisted by H_2O_2 exhibited the enhanced photocatalytic performance for the degradation of hydrolyzed polyacrylamide (HPAM) in visible light irradiation. The conditions such as electrodeposition time of Cu_2O, H_2O_2 dosage, and HPAM concentration were investigated for the degradation of HPAM. The results also showed that the photocatalytic degradation rate of HPAM in the oilfield wastewater under optimal conditions could be 94% within 2 h. Cu_2O/GO@NF can be separated from the system simply and easily, and exhibited significant photocatalytic activity after seven successive recycles, which confirmed that the components and structure were stable during the photocatalytic process.

Keywords: Cuprous oxide; Graphene; Photocatalyst; Degradation; Hydrolyzed polyacrylamide

1. Introduction

Hydrolyzed polyacrylamide (HPAM) has played an important role in enhanced oil recovery applications [1]. Accordingly, produced wastewater containing high concentration of HPAM makes oil into the emulsified oil, which is difficult to be treated by the traditional wastewater treatment methods [2]. Although HPAM is considered as non-toxic, the residual HPAM in oil is easily broken down by physical–chemical factors and its intermediate products are hazardous as their monomer is highly toxic [3]. In recent time, the degradation of HPAM is a much explored area. Many methods have been employed including ultrasonic degradation, thermal degradation, biodegradation, chemical degradation, and photodegradation [4]. Among these methods, the photodegradation is of significant interest for the degradation of various pollutants due to the inexpensive photocatalysts, time-consuming process and an ambient, non-toxicity, and clean condition. However, many

photocatalyst showed the low degradation rate for HPAM, it is very necessary to look for effective materials to deal with HPAM-containing wastewater.

Many metal oxide materials, such as TiO_2 [5], ZnO [6], NiO [7], Cu_2O [8], WO_3 [9], Ag_2O [10], and Bi_2O_3 [11], have increasingly gained attention for photocatalytic degradation of pollutants. As a p-type semiconductor, cuprous oxide has unique optical and electrical properties under visible light, which itself presents as a promising material in many fields, such as solar energy conversion, photocatalytic degradation, catalysis, and sensors [11–14]. However, Cu_2O has some drawbacks in its practical applications, such as the slow electron transfer, rapid electron–hole recombination, and poor photochemical stability [15,16]. In order to enhance the photocatalytic performance of Cu_2O, many works have been concentrated by combining Cu_2O with graphene [15,17–19]. Due to the large surface area and better electrical conductivity, graphene can slow the electron–hole pairs, increase the transfer rate of the photogenerated electrons and surface-adsorbed amount of chemical molecules through π–π interactions, and improve the stability of Cu_2O [20,21]. However, the pulverous

* Corresponding author.

Cu$_2$O/graphene composite is very hard to separate and recycle in the suspending system. Thus, the one-bulk structure is highly appropriate. Some carriers, such as a metal plate and conductive glass, have been researched, but the low specific area restricted their application [22]. Recently, nickel foam (NF) has been widely investigated in some photocatalysts [23–25], owing to its distinguished advantages, such as a unique three-dimensional (3D) scaffold structure, low cost, a big surface area, good structural stability, and so on.

In this paper, Cu$_2$O was composed with GO and NF to get 3D Cu$_2$O/GO@NF photocatalyst by an immersion-electrodeposition method. The 3D Cu$_2$O/GO@ NF composite exhibited higher photocatalytic activities in the degradation of HPAM under visible light irradiation. The enhanced photocatalytic activity was attributed to the synergetic effects including enhanced visible light absorption and effective separation of photogenerated electron–hole pairs. To the best of our knowledge, this is the first time that the prepared 3D Cu$_2$O/GO@NF composite photocatalyst is reported, and this work would put forward an application to deal with high concentration HPAM-containing oilfield wastewater.

2. Materials and methods

2.1. Materials

Graphite powder and copper sulfate pentahydrate were purchased from Sinopharm Chemical Reagent Co., Ltd. (Shanghai, China). Potassium permanganate, sulfuric acid, and hydrogen peroxide were purchased from Xilong Scientific Co., Ltd. (China). Sodium acetate trihydrate were purchased from Shanghai Chemical Reagent Institute Co. Ltd. (Shanghai, China). HPAM was obtained from Daqing Refining & Chemical Company (China). NF was purchased from Changsha Lyrun Material Co., Ltd. (Changsha, China). Oilfield wastewater came from Changqing Oilfield (China).

2.2. Preparation of 3D Cu$_2$O/GO@NF composite

GO@NF was prepared by the immersion method. First, GO was prepared from pure graphite powder by a modified Hummers method. Second, 6 mg of GO were added to 20 mL of distilled water, and the suspension was sonicated for 120 min. Then, after NF (1 cm × 2.5 cm) was placed into the suspension for 5 min, and it was taken out and dried in the air. The 3D Cu$_2$O/GO@NF can be obtained by electrodepositing Cu$_2$O on the GO@NF at –0.22 V for a definite time in 0.10 mol/L CH$_3$COONa and 0.02 mol/L CuSO$_4$ solution (pH = 6.2).

2.3. Characterizations

A Model CHI660A Electrochemistry Workstation (Chenhua Instruments, Shanghai, China) was used for the electrodeposition of Cu$_2$O. A three-electrode system was utilized, where a standard saturated calomel electrode served as the reference electrode, a platinum wire electrode as the auxiliary electrode, and GO@NF as the working electrode. Scanning electron microscopy (SEM) and energy dispersive spectrum (EDS) measurements were carried out with a scanning electron microscope (JEOL JSM-6700 F, Japan). Transmission electron micrographs were recorded on a transmission electron

microscope (TEM; Tecnai G2F20 S-Twin, FEI, USA). Powder X-ray diffraction (XRD) measurements were carried out with a Rigaku X-ray diffractometer (Ricoh Company Ltd., Tokyo, Japan). The UV–vis absorption spectra of HPAM were found on a UV–vis spectrophotometer (UV-2600, Shimadzu Corporation, Japan). Photoluminescence (PL) spectra were acquired by a Lumina Fluorescence Spectrometer (Thermo Scientific, USA). The visible light was provided by the cold light source lamp (9W, Huashuo Lighting Technology Co., Ltd., China).

2.4. Measurement of HPAM concentration

The concentration of HPAM was measured according to Scoggins and Miller [26]. In brief, 50 mL of HPAM solution were prepared and adjusted its pH value (pH = 5) with CH$_3$COONa–CH$_3$COOH buffer solution. Subsequently, 1 mL of Br$_2$/KBr solution was dripped into the HPAM solution and reacted for 10 min. Then, 5 mL of sodium formate solution (1.0 wt%) was added and reacted for 5 min. Then, 5 mL of starch-CdI$_2$ solution was added into the mixture and reacted for 20 min. At the last, the absorbance of the solution was measured by spectrophotometer at maximum absorption wavelength 567 nm with the reference of deionized water (Fig. 1(a)). A calibration curve was obtained in the same condition. The linear calibration curve is $A = 0.00251c + 0.3964$ ($R = 0.9981$) up to 100.0 mg/L (Fig. 1(b)).
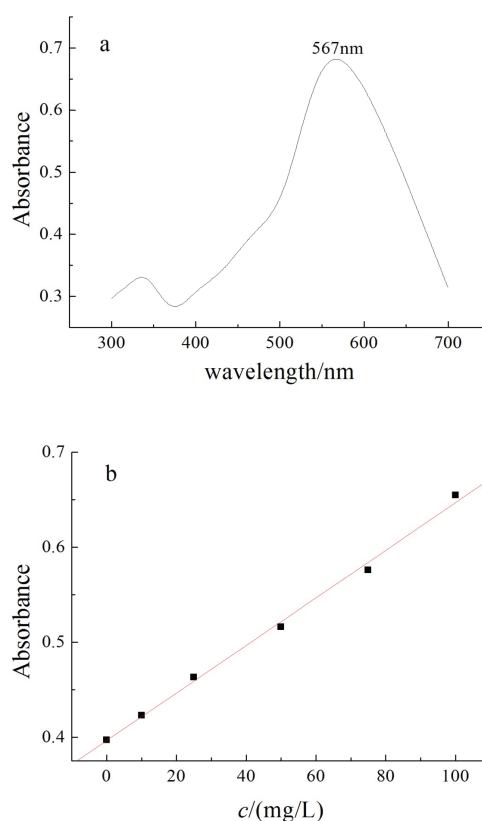

Fig. 1. Absorption spectrum of PAM (a) and a linear calibration curve (b).

2.5. Evaluation of photocatalytic performances

The photocatalytic activities of 3D $Cu_2O/GO@NF$ composite were examined through degradation of HPAM. The 3D $Cu_2O/GO@NF$ composite was placed into 200 mg/L HPAM aqueous solution. Then, the dispersion was kept in dark for 60 min under magnetic stirring to reach the adsorption–desorption equilibrium. HPAM concentrations after irradiation for a definite time were measured. For comparison, the reactions were conducted in the presence of NF or GO@NF and in the absence of any catalyst. The degradation rate of HPAM was obtained by using Eq. (1):

$$R\% = \frac{C_0 - C_t}{C_0} \tag{1}$$

where C_0 and C_t are, respectively, initial concentration and concentration at a definite time. The photodegradation of HPAM follows pseudo-first-order kinetics, which can be reflected in using Eq. (2):

$$\ln\left(\frac{C}{C_0}\right) = -kt \tag{2}$$

where k (min^{-1}) is the degradation rate constant.

3. Results and discussion

3.1. SEM and TEM analysis

SEM and EDS images result of $Cu_2O/GO@NF$ composite are shown in Fig. 2. From Fig. 2(a), 3D, porous, and cross-linked grid structure of NF can be clearly observed. From Fig. 2(b), it is obvious that the skeleton of NF is covered by Cu_2O and GO. From Fig. 2(c), it can be seen that regular octahedral Cu_2O crystals were electrodeposited uniformly on the surface of GO@NF. Cu, O, Ni, and C peaks can be found in the EDS (Fig. 2(d)), which preliminarily confirmed the formation of $Cu_2O/GO@NF$.

Fig. 3 shows the TEM images of GO and Cu_2O/GO. From Fig. 3(a), the thin layer of GO with some wrinkles can be seen clearly. From Fig. 3(b), it is seen that Cu_2O particle is distributed on the graphene surface. These results further affirmed the successful preparation of Cu_2O/GO.

3.2. XRD analysis

XRD patterns of GO@NF and $Cu_2O/GO@NF$ are shown in Fig. 4. Phase peaks at $2\theta = 36.5°$ and $42.4°$ correspond to (111) and (200) planes of the Cu_2O crystal, respectively (JCPDS no. 78-2076). The two characteristic peaks at $2\theta = 44.4°$ and $51.8°$ in the XRD pattern are from the Ni foam (JCPDS no. 65-2865). The absence of diffraction peaks of carbon species is attributed to the low amount and the relatively low diffraction intensity of GO [27].

3.3. PL analysis

The PL analysis can often be used to investigate the extent of the separation of photoinduced electron–hole pairs
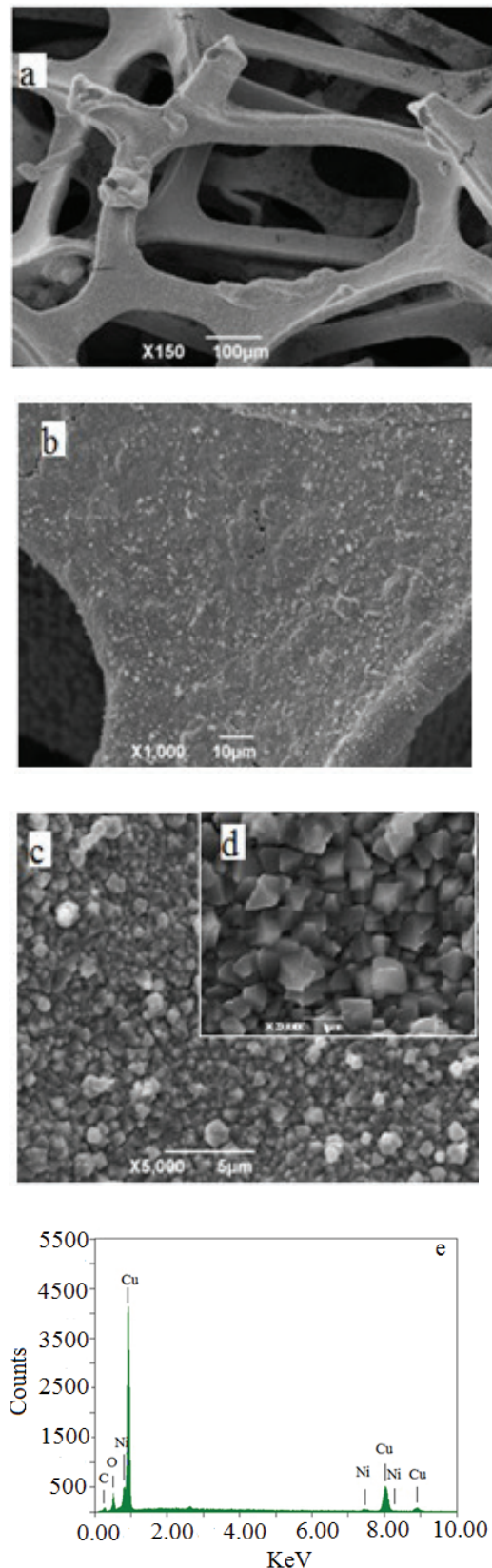

Fig. 2. SEM images of $Cu_2O/GO@NF$ with different magnification (a) 150×, (b) 1,000×, (c) 5,000×, (d) 20,000×, and (e) EDS image of $Cu_2O/GO@NF$.
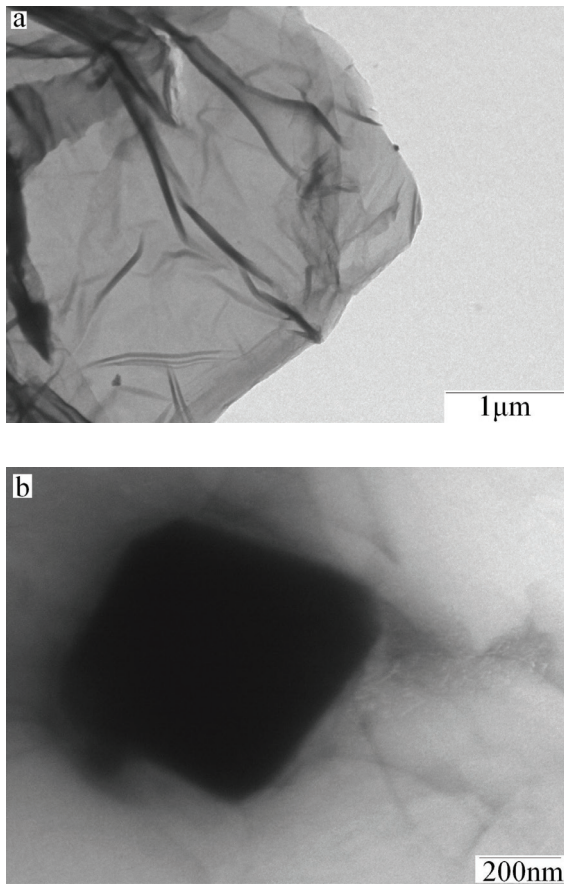
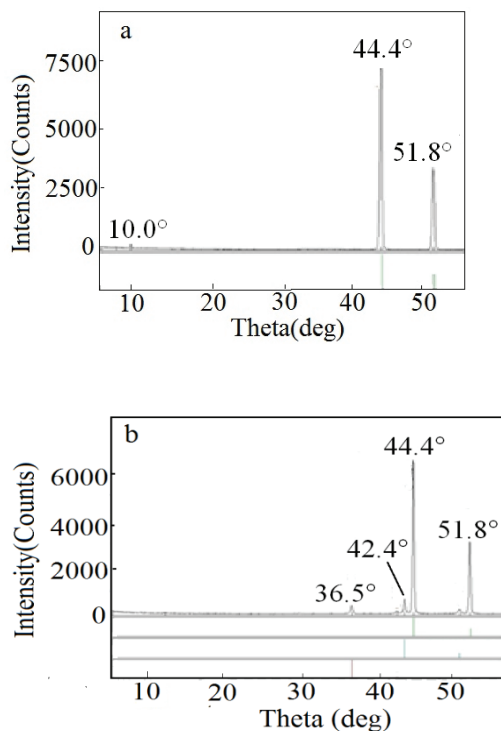Fig. 3. TEM images of GO (a) and Cu_2O/GO (b).

Fig. 4. XRD patterns of (a) GO@NF and (b) Cu_2O/GO@NF.

within an activated photocatalyst [28]. PL arises from the photons, which are produced by the recombination process of electrons and holes after being irradiation [29]. As shown in Fig. 5, NF which was excited at 290 nm showed a typically extensive emission peak at 342 nm. When GO was inserted in the NF, PL intensity decreased. As Cu_2O was electrodeposited on the GO@NF, a significant decrease can be observed at the emission wavelength of 342 nm, which indicated that the recombination of photoinduced electron–hole pairs was inhibited greatly due to the superior electron acceptor ability of the 3D structures, electrical conductivity of Cu_2O/GO@NF.

3.4. Optimization of photocatalytic conditions for Cu_2O/GO@NF

3.4.1. Effect of electrodeposition time of Cu_2O

It is important to control the accounts of Cu_2O on the GO@NF. The accounts of Cu_2O on the GO@NF can be changed by adjusting the electrodeposition time of Cu_2O. In Fig. 6, when H_2O_2 was absent, it can be seen that Cu_2O/GO@NF exhibited excellent photocatalytic activity under visible light irradiation compared with GO@NF and NF,
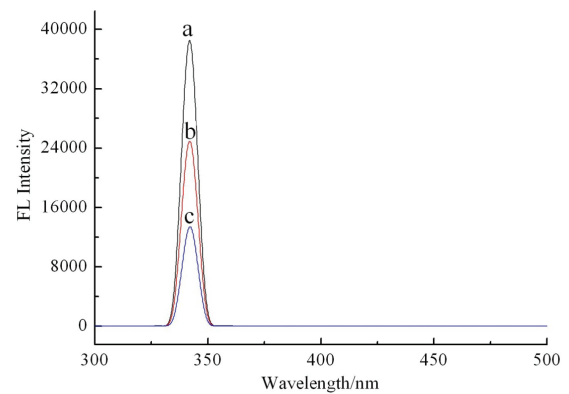

Fig. 5. PL spectra of NF (a), Cu_2O/GO (b), and Cu_2O/GO@NF (c).
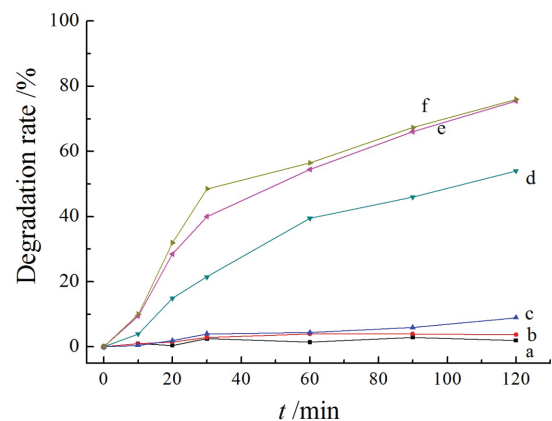

Fig. 6. The effect of electrodeposition time of Cu_2O on the photocatalytic degradation of HPAM (a) without photocatalyst, (b) NF, (c) GO@NF, (d) Cu_2O/GO@NF under the electrodeposition of 30 min, (e) Cu_2O/GO@NF under the electrodeposition of 60 min, and (f) Cu_2O/GO@NF under the electrodeposition of 120 min.

which suggested a synergetic effect between Cu_2O and GO. However, when electrodeposition time of Cu_2O was beyond 60 min, the degradation rate can reach the maximum value up to 76% at 2 h, which indicated the best electrodeposition time of Cu_2O was 60 min.

3.4.2. Effect of H_2O_2 dosage

Fig. 7 shows the effect of H_2O_2 dosage on the photocatalytic degradation of HPAM. From Fig. 7, it can be seen that $Cu_2O/GO@NF$ with H_2O_2 produced a significant acceleration for the photocatalytic degradation of HPAM, which suggested a synergetic effect between $Cu_2O/GO@NF$ and H_2O_2. The reason was that H_2O_2 can react with the electrons of the conduction band of Cu_2O and also produce hydroxyl radicals which were then available to attack HPAM (Eqs. (3)–(7)). However, it should be noted that when the concentration of H_2O_2 was over 18 mol/L, the degradation rate of HPAM decreased. It can be explained that excess H_2O_2 can lead to a decrease in the number of hydroxyl radicals in the solution (Eqs. (8) and (9)) [30]. 18 mol/L was selected as the best H_2O_2 dosage.
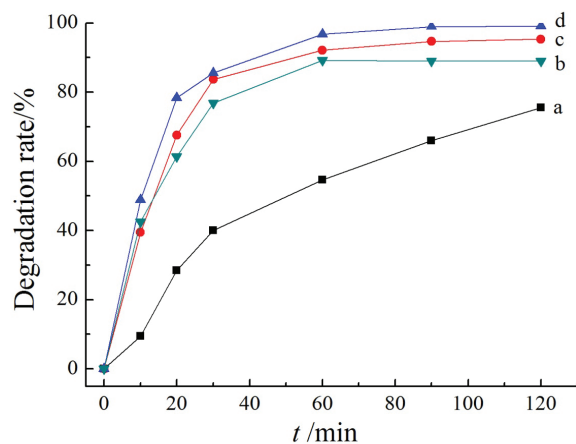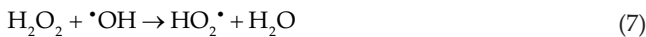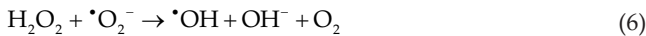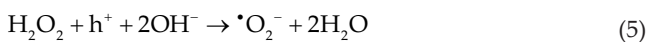
$$Cu_2O \xrightarrow{hv} Cu_2O(h^+, e^-) \tag{3}$$

$$H_2O_2 + e^- \rightarrow {}^\bullet OH + OH^- \tag{4}$$

$$H_2O_2 + h^+ + 2OH^- \rightarrow {}^\bullet O_2^- + 2H_2O \tag{5}$$

$$H_2O_2 + {}^\bullet O_2^- \rightarrow {}^\bullet OH + OH^- + O_2 \tag{6}$$

$$H_2O_2 + {}^\bullet OH \rightarrow HO_2{}^\bullet + H_2O \tag{7}$$

$$H_2O_2 + {}^\bullet OH \rightarrow {}^\bullet OOH + H_2O \tag{8}$$

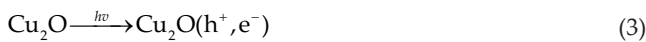$${}^\bullet OOH + {}^\bullet OH \rightarrow O_2 + H_2O \tag{9}$$

Fig. 7. The effect of H_2O_2 dosage on the photocatalytic degradation of PAM (a) 0 mmol/L H_2O_2, (b) 9 mmol/L H_2O_2, (c) 18 mmol/L H_2O_2, and (d) 24 mmol/L H_2O_2.

3.4.3. Effect of initial HPAM concentration

From Fig. 8, it can be observed that the degradation rate of HPAM decreased with increasing initial HPAM concentration in the presence of $Cu_2O/GO@NF$ and 18 mmol/L H_2O_2. Since the number of photons generated and the photocatalyst dosage were constant, the same amount of hydroxyl radicals can be produced in the tests. Hence, an increase in HPAM concentration can result in a decrease in the degradation rate.

3.5. Stability of the $Cu_2O/GO@NF$

The stability of the $Cu_2O/GO@NF$ was investigated by the cyclic use for the degradation of HPAM for 2 h under visible light irradiation with 18 mol/L H_2O_2. The results are presented in Fig. 9. In repeated experiments, $Cu_2O/GO@NF$ was easily recycled by simple washing without any treatment in this process. As shown in Fig. 9, it did not exhibit any significant loss of activity after seven successive cycles, which confirmed the $Cu_2O/GO@NF$ was stable during the photocatalytic degradation process.
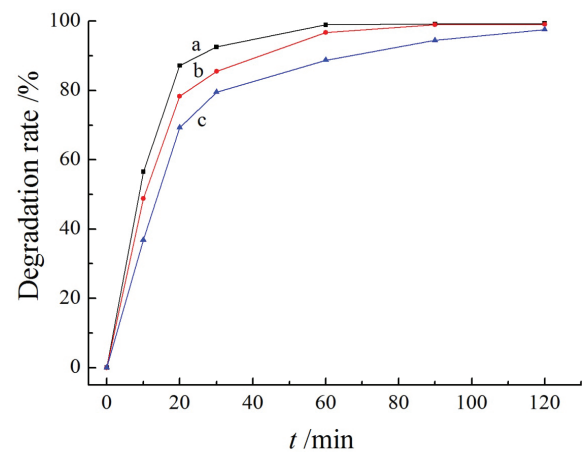

Fig. 8. The effect of initial HPAM concentration on the photocatalytic degradation (a) 100 mg/L HPAM, (b) 200 mg/L HPAM, and (c) 300 mg/L HPAM.
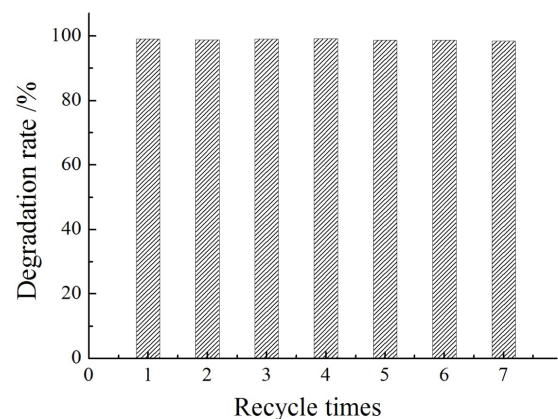

Fig. 9. Cyclic uses of $Cu_2O/GO@NF$ in the photocatalytic degradation of HPAM.

Table 1
Water quality indexes of the oilfield wastewater

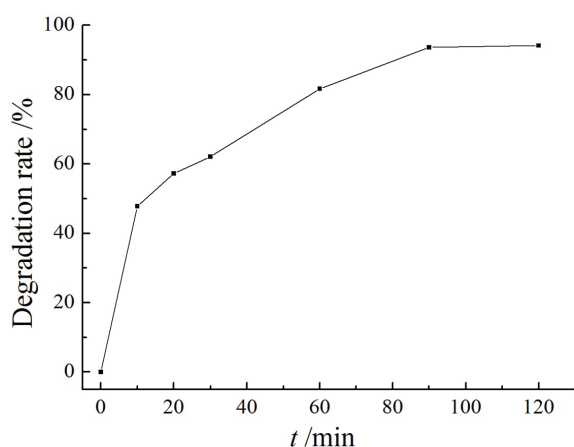| Parameter	Average value	Parameter	Average value
Total suspended solids (mg/L)	117	Mg^{2+} (mg/L)	655.8
pH	6.7	Fe^{3+} (mg/L)	77.4
Cl^- (mg/L)	20,638.8	Fe^{2+} (mg/L)	94.2
Ca^{2+} (mg/L)	6,040.6	HCO_3^- (mg/L)	1,046.0

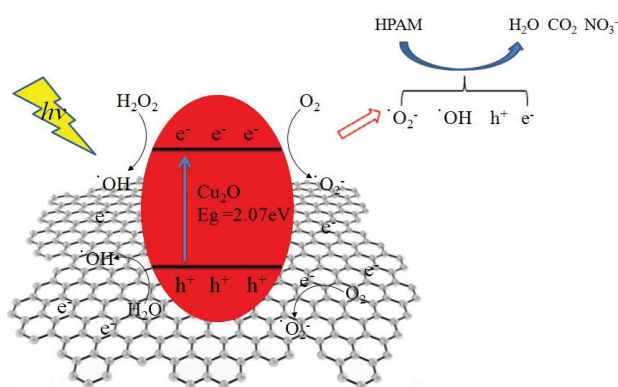Fig. 10. The photocatalytic degradation of HPAM in the oilfield wastewater.

Fig. 11. The proposed mechanism for the photocatalytic degradation of HPAM under visible light irradiation.

Table 2
Comparison with other methods for the degradation of HPAM

Pollutants	Degradation method	Time	Degradation rate (%)	Reference
HPAM	Photodegradation over W/Mo codoped $BiVO_4$	3 h	43	[31]
HPAM	Photoelectrocatalytic degradation with Au/TiO_2	3.5 h	43.84	[32]
HPAM	Biodegradation	3 d	79.4	[33]
HPAM	Mechanical degradation	Unmentioned	42	[34]
HPAM	ZEA advanced oxidation and aerobic biological degradation	43 h	96	[35]
HPAM	Photoelectrocatalytic degradation by $Cu_2O/GO@NF$ and H_2O_2	2 h	94	This work

3.6. Photocatalytical degradation of HPAM in oilfield wastewater

The oilfield wastewater was produced in Changqing Oilfield. Its quality is shown in Table 1. Fig. 10 shows the curve of the degradation of HPAM in the oilfield wastewater which contained 92.3 mg/L HPAM under visible light irradiation with 18 mol/L H_2O_2. Fig. 10 shows that comparing with the degradation of HPAM in distilled water, the degradation rate of HPAM in oilfield wastewater was lower. The reason may be that the suspended matters and high concentration of ions reduced the visible light absorption of $Cu_2O/GO@NF$. However, the degradation rate maintained still at a high level which was 94%. So this technique was capable of the treatment of the oilfield wastewater containing HPAM.

Based on these results, the possible mechanism for photocatalytic degradation of HPAM was proposed over $Cu_2O/GO@NF$ under visible light irradiation in Fig. 11 [2,17]. Cu_2O can be excited under the visible light to produce h^+ and e^-. e^- can react with H_2O_2 and O_2 to generate $\cdot OH$ and superoxide radical anions ($\cdot O_2^-$), respectively. h^+ can combine with H_2O to produce $\cdot OH$. These reactive radical species of $\cdot O_2^-$, $\cdot OH$, h^+, and e^- can degrade HPAM into NO_3^-, H_2O, and CO_2.

3.7. Comparison with other methods for the degradation of HPAM

Comparison with other methods for the degradation of HPAM is listed in Table 2. From Table 2, it can be seen that the degradation rate or degradation time was superior to the literatures, which showed the perfect photocatalytic activity of $Cu_2O/GO@NF$ and satisfactory performance for the photocatalytical degradation of HPAM. So, $Cu_2O/GO@NF$ had the potential application for the photocatalytical degradation of HPAM in the oilfield wastewater.

4. Conclusions

As-prepared 3D $Cu_2O/GO@NF$ composite exhibited high photocatalytic activity of HPAM under the visible light. Cu_2O was a visible light active ingredient of $Cu_2O/GO@NF$, in which porous GO@NF contributed to enhance the electron–hole separation for the improvement of the photocatalytic activity of Cu_2O. The synergetic effect between Cu_2O and H_2O_2 was found to enhance the degradation rate obviously. Optimal conditions for the photocatalytic degradation of 200 mg/L HPAM are 60 min of the electrodeposition time of Cu_2O, 18 mmol/L of H_2O_2 and 120 min of visible light irradiation. In addition, 3D $Cu_2O/GO@NF$ composite exhibited an outstanding stability after seven recycles. Therefore, $Cu_2O/GO@NF$ can be a good candidate for application in environmental purification.

Acknowledgments

References

[1] A.M. Mansour, R.S. Al-Maamari, A.S. Al-Hashmi, A. Zaitoun, H. Al-Sharji, In-situ rheology and mechanical degradation of EOR polyacrylamide solutions under moderate shear rates, J. Pet. Sci. Eng., 115 (2014) 57–65.

[2] X.S. Rong, F.X. Qiu, C. Zhang, L. Fu, Y.Y. Wang, D.Y. Yang, Preparation of Ag-AgBr/TiO_2-graphene and its visible light photocatalytic activity enhancement for the degradation of polyacrylamide, J. Alloys Compd., 639 (2015) 153–161.

[3] X.H. Dai, F. Luo, J. Yi, Q.B. He, B. Dong, Biodegradation of polyacrylamide by anaerobic digestion under mesophilic condition and its performance in actual dewatered sludge system, Bioresour. Technol., 153 (2014) 55–61.

[4] L. Yi, K.Z. Li, D.X. Liu, Degradation of polyacrylamide: a review, Adv. Mater. Res., 800 (2013) 411–416.

[5] B.C. Qiu, M.Y. Xing, J.L. Zhang, Mesoporous TiO_2 nanocrystals grown in situ on graphene aerogels for high photocatalysis and lithium-ion batteries, J. Am. Chem. Soc., 136 (2014) 5852–5855.

[6] D. Liu, Y.H. Lv, M. Zhang, Y.F. Liu, Y.Y. Zhu, R.L. Zong, Y.F. Zhu, Defect-related photoluminescence and photocatalytic properties of porous ZnO nanosheets, J. Mater. Chem. A, 2 (2014) 15377–15388.

[7] F. Motahari, M.R. Mozdianfard, F. Soofivand, M. Salavati-Niasari, NiO nanostructures: synthesis, characterization and photocatalyst application in dye wastewater treatment, RSC Adv., 4 (2014) 27654–27660.

[8] W.C. Huang, L.M. Lyu, Y.C. Yang, M.H. Huang, Synthesis of Cu_2O nanocrystals from cubic to rhombic dodecahedral structures and their comparative photocatalytic activity, J. Am. Chem. Soc., 134 (2012) 1261–1267.

[9] J. Kim, C.W. Lee, W. Choi, Platinized WO_3 as an environmental photocatalyst that generates OH radicals under visible light, Environ. Sci. Technol., 44 (2010) 6849–6854.

[10] X.F. Wang, S.F. Li, H.G. Yu, J.G. Yu, S.W. Liu, Ag_2O as a new visible-light photo catalyst: self-stability and high photocatalytic activity, Chem. Eur. J., 17 (2011) 7777–7780.

[11] L. Zhang, H. Wang, Cuprous oxide nanoshells with geometrically tunable optical properties, ACS Nano, 5 (2011) 3257–3267.

[12] F.X. Gao, X.D. Wang, D.Z. Wu, Design and fabrication of bifunctional microcapsules for solar thermal energy storage and solar photocatalysis by encapsulating paraffin phase change material into cuprous oxide, Sol. Energy Mater. Sol. Cells, 168 (2017) 146–164.

[13] L. Wu, Y.L. Wu, S. Jin, L. Zhang, Z.P. Xun, Gas sensitivity and photocatalytic performance of cuprous oxide with novel morphologies, Chem. Phys. Lett., 662 (2016) 47–51.

[14] W.C.J. Ho, Q. Tay, H. Qi, Z.H. Huang, J. Li, Z. Chen, Photocatalytic and adsorption performances of faceted cuprous oxide (Cu_2O) particles for the removal of methyl orange (MO) from aqueous media, Molecules, 22 (2017) 677.

[15] F.G. Han, H.P. Li, J. Yang, X.D. Cai, L. Fu, One-pot synthesis of cuprous oxide-reduced graphene oxide nanocomposite with enhanced photocatalytic and electrocatalytic performance, Physica E, 77 (2016) 122–126.

[16] X.Q. Liu, Z. Li, W. Zhao, C.X. Zhao, Y. Wang, Z.Q. Lin, A facile route to the synthesis of reduced graphene oxide-wrapped octahedral Cu_2O with enhanced photocatalytic and photovoltaic performance, J. Mater. Chem. A, 3 (2015) 19148–19154.

[17] X.Q. An, K. Li, J.W. Tang, Cu_2O/reduced graphene oxide composites for the photocatalytic conversion of CO_2, Chem. Sus. Chem., 7 (2014) 1086–1093.

[18] J. Liu, J. Ke, D.G. Li, H.Q. Sun, P. Liang, X.G. Duan, W.J. Tian, M.O. Tadé, S.M. Liu, S.B. Wang, Oxygen vacancies in shape controlled Cu_2O/reduced graphene oxide/In_2O_3 hybrid for promoted photocatalytic water oxidation and degradation of environmental pollutants, ACS Appl. Mater. Interfaces, 9 (2017) 11678–11688.

[19] Y.H. Zheng, Z. Wang, F. Peng, A.W. Wang, X.D. Cai, L. Fu, Growth of Cu_2O nanoparticle on reduced graphene sheets with high photocatalytic activity for degradation of Rhodamine B, Fullerenes Nanotubes Carbon Nanostruct., 4 (2016) 149–153.

[20] Q.J. Xiang, J.G. Yu, M. Jaroniec, Graphene-based semiconductor photocatalysts, Chem. Soc. Rev., 41 (2012) 782–796.

[21] P. Tran, S. Batabyal, S. Pramana, J. Barber, L. Wong, S. Loo, A cuprous oxide-reduced graphene oxide (Cu_2O-rGO) composite photocatalyst for hydrogen generation: employing rGO as an electron acceptor to enhance the photocatalytic activity and stability of Cu_2O, Nanoscale, 4 (2012) 3875–3878.

[22] M. Yu, Y.X. Ma, J.H. Liu, X.J. Li, S.M. Li, S.Y. Liu, Sub-coherent growth of ZnO nanorod arrays on three-dimensional graphene framework as one-bulk high-performance photocatalyst, Appl. Surf. Sci., 390 (2016) 266–272.

[23] Y. Xue, R. Su, G. Zhang, Q. Wang, P. Wang, W. Zhang, Z.H. Wang, Visible light responsive Fe–ZnS/nickel foam photocatalyst with enhanced photocatalytic activity and stability, RSC Adv., 6 (2016) 93370–93373.

[24] Q. Zhang, F. Li, X.Y. Chang, D.L. He, Comparison of nickel foam/Ag-supported ZnO, TiO_2, and WO_3 for toluene photodegradation, Mater. Manuf. Processes, 29 (2014) 789–794.

[25] R. Azimirad, S. Safa, Preparation of three dimensional graphene foam-WO_3 nanocomposite with enhanced visible light photocatalytic activity, Mater. Chem. Phys., 162 (2015) 686–691.

[26] M.W. Scoggins, J.W. Miller, Spectrophotometric determination of water soluble organic amides, Anal. Chem., 47 (1975) 152–154.

[27] J. Lee, K. You, C. Park, Highly photoactive, low bandgap TiO_2 nanoparticles wrapped by graphene, Adv. Mater., 24 (2012) 1084–1088.

[28] M. Cao, P. Wang, Y. Ao, C. Wang, J. Hou, J. Qian, Photocatalytic degradation of tetrabromobisphenol A by a magnetically separable grapheme-TiO_2 composite photocatalyst: mechanism and intermediates analysis, Chem. Eng. J., 264 (2015) 113–124.

[29] S.D. Perera, R.G. Mariano, K. Vu, N. Nour, O. Seitz, Y. Chabal, K.J. Balkus Jr., Hydrothermal synthesis of grapheme-TiO_2 nanotube composites with enhanced photocatalytic activity, ACS Catal., 2 (2012) 949–956.

[30] S. Parra, V. Nadtotechenko, P. Albers, J. Kiwi, Discoloration of azo-dyes at biocompatible pH-values through an Fe-histidine complex immobilized on Nafion via Fenton-like processes, J. Phys. Chem. B, 108 (2004) 4439–4448.

[31] Y. Zhou, W. Li, W. Wan, R. Zhang, Y. Lin, W/Mo co-doped $BiVO_4$ for photocatalytic treatment of polymer-containing wastewater in oilfield, Superlattices Microstruct., 82 (2015) 67–74.

[32] D. Gu, Y. Wang, Z.D. Li, Y. Liu, B.H. Wang, H.J. Wu, UV-light aided photoelectrochemical synthesis of Au/TiO_2 NTs for photoelectrocatalytic degradation of HPAM, RSC Adv., 6 (2016) 63711–63716.

[33] J.H. Liu, J.W. Ren, R.D. Xu, B. Yu, J. Wang, Biodegradation of partially hydrolyzed polyacrylamide by immobilized bacteria isolated from HPAM-containing wastewater, Environ. Prog. Sustain. Energy, 35 (2016) 1344–1352.

[34] A.R. Al Hashmi, R.S. Al Maamari, I.S. Al Shabibi, A.M. Mansoor, A. Zaitoun, H.H. Al Sharji, Rheology and mechanical degradation of high-molecular-weight partially hydrolyzed polyacrylamide during flow through capillaries, J. Pet. Sci. Eng., 105 (2013) 100–106.

[35] M. Lu, X.F. Wei, Treatment of oilfield wastewater containing polymer by the batch activated sludge reactor combined with a zerovalent iron/EDTA/air system, Bioresour. Technol., 102 (2011) 2555–2562.